ACS APPLIED MATERIALS & INTERFACES

Research Article

www.acsami.org

$CuInS_2$ Nanocrystals/PEDOT:PSS Composite Counter Electrode for Dye-Sensitized Solar Cells

Zhongyi Zhang,[†,‡,⊥] Xiaoying Zhang,[†,⊥] Hongxia Xu,[†] Zhihong Liu,[†] Shuping Pang,[†] Xinhong Zhou,[§] Shanmu Dong,[†] Xiao Chen,[†] and Guanglei Cui*[,†]

[†]Qingdao Institute of Bioenergy and Bioprocess Technology, Chinese Academy of Sciences, Qingdao 266101, People's Republic of China

[‡]College of Chemistry and Chemical Engineering, Qingdao University, Qingdao 266071, People's Republic of China

[§]Qingdao University of Science and Technology, Qingdao 266042, People's Republic of China

Supporting Information

ABSTRACT: An inorganic/organic nanocomposite comprised of $CuInS_2$ nanocrystals and poly(styrenesulfonate)-doped poly(3,4-ethylenedioxythiophene) (CIS/PEDOT:PSS) was explored as a promising candidate for the counter electrode (CE) in dye-sensitized solar cells (DSCs). Cyclic voltammetry measurements confirmed that this composite electrode exhibited better catalytic activity compared with pristine $CuInS_2$ or PEDOT:PSS electrode. Electrochemical impedance spectroscopy revealed that the composite film constitutes a three-dimensional catalytic network. The DSC using this composite CE can yield 6.50% photoelectric conversion efficiency, which is comparable to that of the conventional platinum CE (6.51%) and better than that of the pristine $CuInS_2$ (5.45%) or PEDOT:PSS (3.22%) electrode.

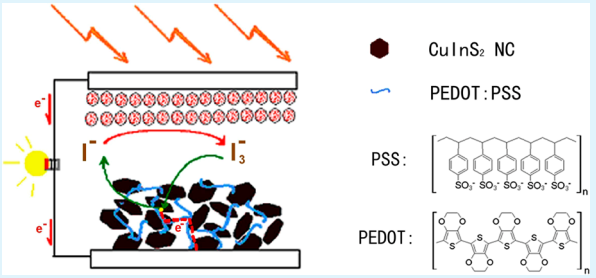

KEYWORDS: *counter electrode, $CuInS_2$, poly(styrenesulfonate)-doped poly(3,4-ethylenedioxythiophene), dye-sensitized solar cells, composite film*

1. INTRODUCTION

Dye-sensitized solar cells (DSCs) have attracted extensive interest for scientific research around the world[1−4] because of the advantages of relatively low cost and the possibility of mechanical flexibility and assembly in large scale.[5−7] The standard DSC was composed of a porous structured oxide film, adsorbed dye molecules as the photosensitized anode, a liquid electrolyte traditionally containing I^-/I_3^- as redox couples, and a platinum counter electrode (CE).[8,9] Among them, the CE collects electrons from the external circuit to the redox electrolyte and catalyzes the reduction of triiodide to iodide ions, which makes the cell a complete circuit. Therefore, the ideal CE materials should possess high electrical conductivity as well as superior electrocatalytic activity in order to minimize the energy losses. Usually, the CEs of DSCs were fabricated by loading platinum on fluorine-doped tin oxide (FTO) glass. The high cost and corrosion of platinum in triiodide-containing solutions necessitate the development of alternative materials.[10] Therefore, many alternative electrodes have been reported, such as carbon-based materials,[11−13] conducting polymers[14−16] and metallic nanomaterials.[17−22]

Transition-metal sulfides have attracted extensive investigation because of their unique catalytic and electrical characteristics.[23] Some metal sulfides, such as CoS, NiS, and WS_2, were reported to exhibit distinct catalytic activities, as the CEs in DSCs.[19−22] Recently, multimetal sulfide was reported to exhibit excellent performance, even surpassing platinum-based CEs in DSCs.[24] The higher catalytic activity may originate from the synergistic mechanism of various metal elements. Nevertheless, the related literature on multimetal sulfide-based CEs is still relatively rare. $CuInS_2$ as one of the typical bimetal sulfides has garnered great interest in recent years because of its promise for photovoltaic applications.[25−27] However, to the best of our knowledge, the use of $CuInS_2$ as potential substitutes for CEs of DSCs has not yet been reported and rare studies have centered on its electrocatalytic activity for use in CEs of DSCs. Herein, we demonstrate that the as-prepared $CuInS_2$ nanocrystals (NCs) have excellent catalytic activity for triiodide reduction reaction. In order to further improve their adhesion to the substrate, those $CuInS_2$ NCs were incorporated with conducting polymers (PEDOT:PSS) to constitute an inorganic/organic nanocomposite CE, which also endows an effective combined network of both high electrical conductivity and superior electrocatalytic activity. With the synergistic catalytic effect, this inorganic/organic nanocomposite CE resulted in a better catalytic performance than pristine $CuInS_2$ or PEDOT:PSS electrode. The study in this work

Received: August 30, 2012
Accepted: October 17, 2012
Published: October 17, 2012

may pave a new pathway to explore highly efficient materials for CEs.

2. EXPERIMENTAL DETAILS

Materials. Copper(I) chloride (Alfa, 99.999%), indium(III) chloride (Alfa, 99.99%), 3-mercapto-1,2-propanediol (alfa, >90%), oleyamine (OLA) (Aldrich, 70%), and poly(styrenesulfonate)-doped poly(3,4-ethylenedioxythiophene) (Aldrich, containing 2.6% PEDOT and PSS 2.2% in aqueous solution) were used as purchased without further purification.

Synthesis of $CuInS_2$ NCs. In a typical synthesis, CuCl (0.5 mmol) and $InCl_3$ (0.5 mmol) were mixed with 3-mercapto-1,2-propanediol (0.6 g) in a 50 mL three-necked flask, followed by the addition of 20 mL of OLA. The mixture was then continuously degassed for 30 min and filled with argon. After that, the solution was heated to 240 °C and kept for 60 min. Subsequently, the solution was cooled to room temperature and then an excess of ethanol was added. The formed precipitate was centrifuged and washed with ethanol several times and subsequently dried in 70 °C to obtain high-purity $CuInS_2$ NCs.

Preparation of CEs. A $CuInS_2$/PEDOT:PSS nanocomposite CE (CIS/PEDOT:PSS CE) was typically prepared by dispersing $CuInS_2$ powder (0.2 g) in a PEDOT:PSS aqueous solution (0.40 g, solid content = 4.8%) and sonicating for 30 min to form a well-dispersed composite solution. The composite solution was drop-cast onto FTO glass, naturally dried to evaporate water, and subsequently sintered at 70 °C for 2 h at an ambient atmosphere. Consequently, the as-prepared nanocomposite film was calculated to contain about 6% PEDOT:PSS. A CE of pristine $CuInS_2$ (CIS CE) was prepared by drop casting 0.5 g mL^{-1} of a $CuInS_2$ NC dispersion (in toluene) on the FTO conductive glass followed by drying to remove the solvent (toluene) and annealing at 350 °C for 30 min under the protection of argon. The mirrorlike Pt-FTO electrode (Pt-FTO CE) was obtained by electrodepositing a platinum layer on the surface of FTO glass. The thickness of the platinum film is about 70 nm.

Fabrication of DSCs. A dye-sensitized porous TiO_2 film was prepared by loading a TiO_2 slurry (Dalian HeptaChroma SolarTech Co., Ltd., China) layer onto FTO glass by the doctor-blading technique. After calcination at 450 °C for 30 min, the TiO_2 film was immersed in a 3×10^{-4} M ethanol solution of ruthenium 535 bis-TBA (N719, Solaronix SA) for 24 h, and then the dye-sensitized TiO_2 film was washed with anhydrous ethanol and dried in moisture-free air. Finally, the dye-sensitized TiO_2 photoanode and the as-fabricated CE were assembled together. The liquid electrolyte, which is composed of 0.5 M LiI, 0.6 M 1-propyl-2,3-dimethylimidazolium iodide, 0.05 M I_2, and 0.5 M 4-*tert*-buylpyridine with acetonitrile as the solvent, was then injected between the two electrodes.

Characterization. Scanning electron microscopy (SEM) images and an energy-dispersive spectrometry (EDS) spectrum were acquired using a Hitachi S-4800 field-emission electron microscope. X-ray diffraction (XRD) measurements were carried out on a Bruker D8 ADVANCE X-ray diffractometer. The current density−voltage (J−V) characteristics of DSCs were measured under 100 mW cm^{-2} irradiation (1 sun calibrated beforehand by a standard silicon solar cell). The irradiation was from a 300 W solar simulator (Newport, RI). Cyclic voltammetry (CV) was carried out in a three-electrode system in an acetonitrile solution of 0.1 M $LiClO_4$, 10 mM LiI, and 1 mM I_2 at a scan rate of 50 mV s^{-1}. Platinum served as a CE, and the Ag/Ag^+ couple was used as a reference electrode. Electrochemical impedance spectroscopy (EIS) of the CEs was recorded using a Zennium electrochemical workstation and performed on dummy cells with a symmetric sandwich-like structure between two identical electrodes, that is, CE/electrolyte/CE. The CEs used for testing in this paper are consistent with equal area. The electrolyte is similar to the one used for fabricating the DSCs. The frequency range was varied from 100 kHz to 100 mHz.

3. RESULTS AND DISCUSSION

$CuInS_2$ NCs were synthesized via a facile solution-based route at 240 °C. SEM images (Figure S1a,b in the Supporting Information, SI) show that the as-prepared $CuInS_2$ NCs are of hexagonal-plate morphologies with average diameter and thickness of ∼200 and ∼50 nm, respectively. XRD patterns (Figure S1c in the SI) identify that $CuInS_2$ NCs are indexed to wurtzite crystal structure, which agrees well with other reports.[25] The chemical composition of the resultant NCs was determined by EDS, which reveals that the atomic ratio of Cu:In:S in the obtained NCs is 1:1:2 (Figure S1d in the SI). Parts a and b of Figure 1 show the SEM images of a $CuInS_2$/PEDOT:PSS nanocomposite. It is shown that PEDOT:PSS agglomerated at the grain boundaries of NCs and interconnected the NCs together. The thickness of the film was controlled at about 13 μm (shown in Figure 1c) and closely contacted with the surface of FTO glass (shown in Figure 1d), as is also schematically illustrated in Figure S3 in the SI.

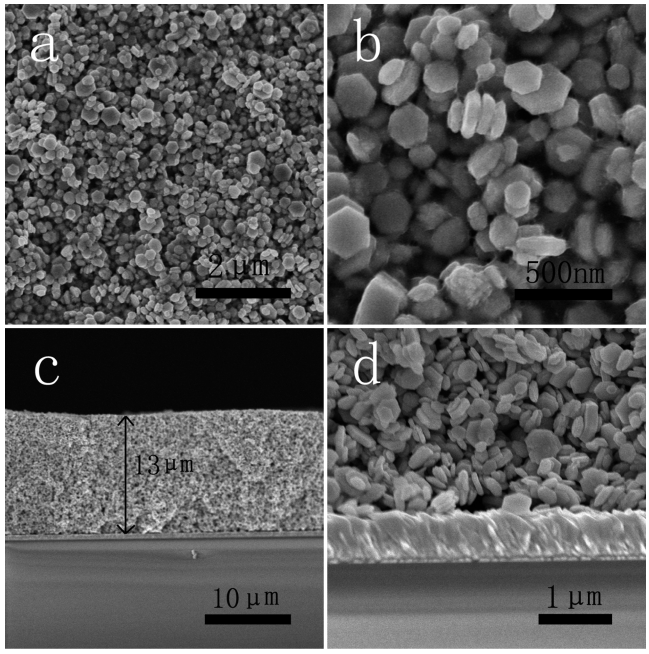

Figure 1. (a) Typical SEM image and (b) its enlarged image of a $CuInS_2$ NCs/PEDOT:PSS nanocomposite. (c) Cross-sectional view of the $CuInS_2$ NCs/PEDOT:PSS nanocomposite electrode and (d) the enlarged image of the contact area with the front of FTO glass.

Figure 2 presents the current density−voltage (J−V) characteristic curves of DSCs based on different CEs, and the detailed photovoltaic parameters are summarized in Table 1. The pristine $CuInS_2$ electrode (CIS CE) achieved a reasonable conversion efficiency (η) of 5.45% and a relatively lower short-circuit current density (J_{sc}). The pristine PEDOT:PSS electrode (PEDOT:PSS CE), however, gained a low η of 3.22% mainly because of a lower fill factor (FF) of 43.7%. In comparison, the nanocomposite electrode (CIS/PEDOT:PSS CE) exhibited a larger photocurrent density (J_{sc} = 16.0 mA cm^{-2}) and induced a higher η of 6.50%, which is comparable to that of Pt-FTO CE (6.51%). Figure S2 in the SI also shows the J−V curves of the CIS/PEDOT:PSS CEs with varying amounts of PEDOT:PSS. It can be seen that, with the concentration of PEDOT:PSS in the range of 2−6% (of the total weight of the composite film), the CEs can yield an efficiency comparable to that of the expensive Pt-FTO CE. All results confirmed that this nanocomposite can greatly improve the performance of CEs.

dx.doi.org/10.1021/am3018338 | ACS Appl. Mater. Interfaces 2012, 4, 6242−6246

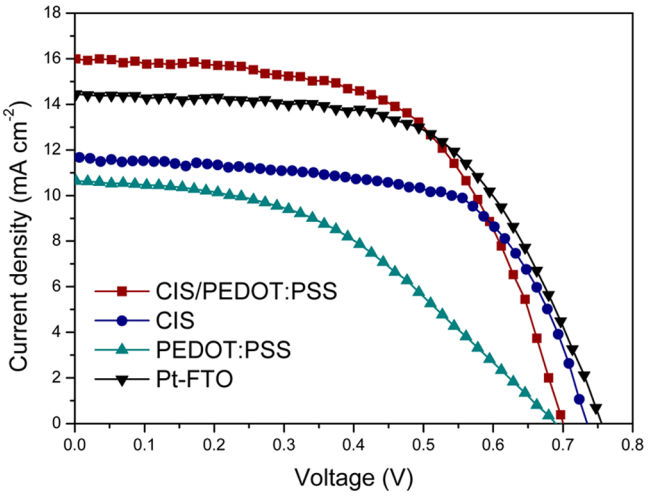

Figure 2. *J*–*V* curves of the DSCs with different CEs under AM 1.5 solar simulator illumination at 100 mW cm^{-2}. CIS/PEDOT:PSS CE: based on the $CuInS_2$ NCs/PEDOT:PSS nanocomposite electrode. CIS CE: based on the pristine $CuInS_2$ NCs. PEDOT:PSS CE: based on the pristine PEDOT:PSS.

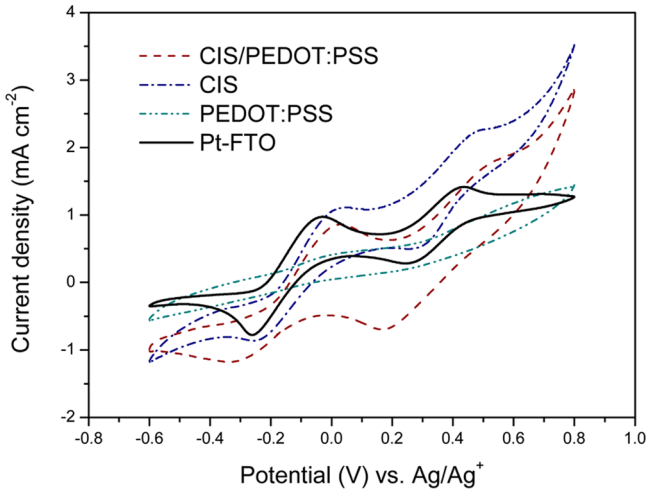

Figure 3. Cyclic voltammograms of iodide species of various CEs with a measured scan rate of 50 mV s^{-1} (the electrolyte is an acetonitrile solution of 0.1 M $LiClO_4$, 10 mM LiI, and 1 mM I_2).

In order to investigate the catalytic mechanism, CV was conducted. Figure 3 shows the CV curves of iodide species for different electrodes. Two typical pairs of oxidation/reduction peaks are clearly observed. The pair at the relatively negative potential is assigned to the redox reaction (1), and the one at the positive potential is assigned to the redox reaction (2) according to the literature.[17]

$$I_3^- + 2e^- \rightleftharpoons 3I^- \quad (1)$$

$$3I_2 + 2e^- \rightleftharpoons 2I_3^- \quad (2)$$

As for pristine CIS CE, the cathodic current densities for both reactions (1) and (2) are comparable to that of Pt-FTO CE, which indicates the excellent catalytic activity of $CuInS_2$ NCs. For the pristine PEDOT:PSS CE, no clear reduction peak appeared, indicating that the reduction reaction rate is very slow on the PEDOT:PSS electrode. In the case of the nanocomposite electrode, despite the reduction peaks moving toward a more negative potential, the integration area of the two reduction peaks becomes larger. Compared with the reduction peak of reaction (1), the current density of reaction (2) was more significantly increased. Because these two equilibrium reactions are in series with each other, the improved catalytic activity for reaction (2) also can accelerate the reaction rate of the composite CE in triiodide reduction corresponding eq 1. Therefore, the nanocomposite electrode comprising $CuInS_2$ NCs incorporated with PEDOT:PSS renders a synergistic catalytic effect compared with either a pristine $CuInS_2$ or PEDOT:PSS electrode.

To further elucidate the electrochemical characteristics of CEs, EIS measurements were performed on dummy cells with a symmetric sandwich-like structure between two identical electrodes, that is, CE/electrolyte/CE.

Figure 4 shows the Nyquist plots using different CEs. It was shown that, for CIS CE and CIS/PEDOT:PSS CE, three semicircles are visible, which was reported to be characteristic of porous CEs.[11,18] This result also corroborates the existence of a three-dimensional (3D) catalytic network that was assembled in the composite film. The Nernst diffusion impedance of the redox couple in the channels between NCs resulted in the second semicircle. Accordingly, the equivalent circuit is illustrated in the inset of Figure 4. According to

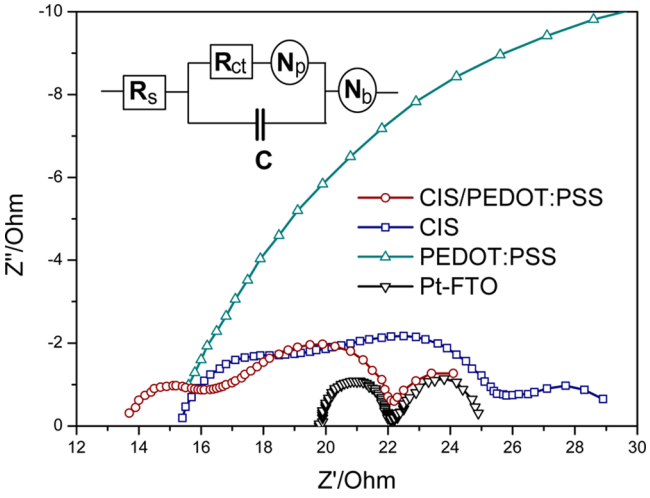

Figure 4. Nyquist plots for different CEs. The test was performed with the symmetrical cells fabricated with two identical electrodes.

Table 1. Photovoltaic Performance of DSCs with Different CEs and EIS Parameters of the Dummy Cell Assembled with Two Identical CEs

CE	V_{oc}/V	J_{sc} /mA cm^{-2}	FF/%	η/%	R_s/Ω	R_{ct}/Ω	C/μF	N_p/Ω	N_b/Ω
CIS/PEDOT:PSS	0.70	16.0	58.1	6.50	14.02	2.21	4.90	5.32	3.25
CIS	0.74	11.6	63.7	5.45	15.76	3.50	3.78	5.67	3.46
PEDOT	0.69	10.7	43.7	3.22	15.65	23.79	41.77	54.59	20.23
Pt-FTO	0.76	14.4	59.8	6.51	19.82	1.81	13.71	0.44	2.81

dx.doi.org/10.1021/am3018338 | ACS Appl. Mater. Interfaces 2012, 4, 6242–6246

previous literature,[11,18] we attribute the first semicircle at the high-frequency region to the charge-transfer resistance (R_{ct}) and the double-layer capacitance (C) of the electrode surface. The middle-frequency semicircle corresponds to the Nernst diffusion impedance (N_p), resulting from diffusion through the 3D electrode. As in the traditional approach, the low-frequency semicircle is determined by bulk Nernst diffusion (N_b). Additionally, the intercept on the real axis (high frequency) can be assigned to the series resistance (R_s).[18] The EIS spectrum analytical results of R_{ct} and R_s are summarized in Table 1. It was generally recognized that a smaller R_{ct} represents a higher electrocatalytic activity toward redox electrolyte.[17] R_{ct} of a pristine PEDOT:PSS electrode (23.79 Ω) is distinctly larger than the other three CEs, which is in accordance with its inferior FF (43.7%). R_{ct} values of CIS and CIS/PEDOT:PSS are 3.50 and 2.21 Ω, which are close to that of the platinum electrode, indicating that $CuInS_2$ NCs and its composite have a superior electrocatalytic activity. The series resistance R_s values of CIS and PEDOT:PSS are 15.76 and 15.65 Ω, respectively. For the composite electrode CIS/PEDOT:PSS, R_s is 14.02 Ω, which is smaller than those of either CIS or PEDOT:PSS CEs. The smaller R_s value of CIS/PEDOT:PSS CE may originate from the conducting polymers, which improved the electronic conductivity and adhesion between FTO glass and the catalytic film. The overall impedance of the composite electrode is very close to that of Pt-FTO, resulting in a comparable photovoltaic performance.

Figure 5 depicts the Tafel polarization curves of the dummy cells based on different electrodes, which shows the logarithmic

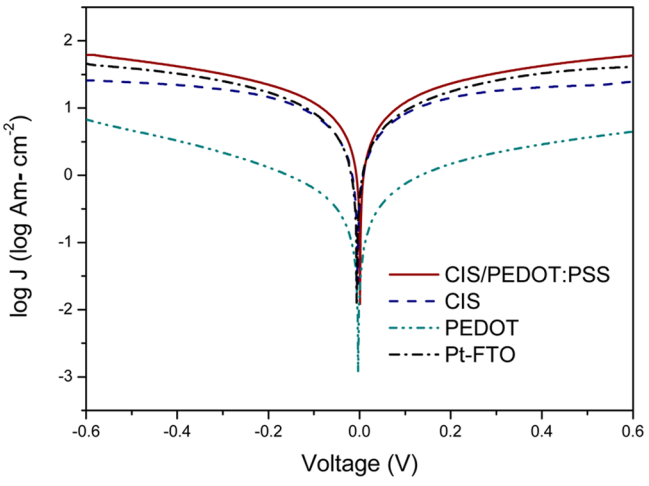

Figure 5. Tafel curves of the symmetrical dummy cells fabricated with various electrodes.

current density (log J) as a function of the voltage. The exchange current can be calculated from the intersection of the linear anodic and cathodic curves. The CIS/PEDOT:PSS electrode exhibits a large exchange current density J_0 compared with that of Pt-FTO. It is also shown that incorporating PEDOT:PSS with $CuInS_2$ NCs also improves the limiting diffusion current density (J_{lim}). This confirms that the catalytic activity of the CIS/PEDOT:PSS electrode is sufficient to catalyze the reduction of triiodide to iodide. A pristine CIS CE shows an exchange current density J_0 and a relatively smaller J_{lim} comparable to those of the Pt-FTO electrode. In the case of a pristine PEDOT:PSS CE, the much smaller J_{lim} and J_0 represent their relatively lower catalytic activities. At the same time, J_{lim} obtained from the Tafel polarization curves of the dummy cells depends on the diffusion coefficient of the triiodide/iodide redox couple in the DSC system. As a result, it was also illustrated that the CIS/PEDOT:PSS electrode ensures a higher diffusion coefficient of the triiodide/iodide redox couple than the other three electrodes. Therefore, the excellent photovoltaic performance of the CIS/PEDOT:PSS electrode is in agreement with the EIS and Tafel polarization results on the whole.

4. CONCLUSIONS

The $CuInS_2$/PEDOT:PSS composite CEs were prepared by the incorporation of high-purity $CuInS_2$ NCs with PEDOT:PSS and exhibited much higher catalytic activity for the reduction reaction than a pristine $CuInS_2$ or PEDOT:PSS electrode. Consequently, a much better conversion efficiency of 6.50% was achieved, which is already comparable to that of the high-cost Pt-FTO electrode (6.51%). On the basis of analysis of EIS, CV curves, and Tafel polarization, it was shown that the CIS/PEDOT:PSS CEs show excellent electrode performance. Additionally, this type of inorganic/organic composite electrode is also feasible to apply in flexible substrates. It was expected that the exploration may extend the feasibility of an inorganic/organic composite electrode as promising low-cost CEs for DSCs.

■ ASSOCIATED CONTENT

Ⓢ Supporting Information

Typical SEM, XRD, and EDS of the as-prepared $CuInS_2$ NCs and photovoltaic performance of DSCs using $CuInS_2$/PEDOT:PSS CEs with varying amounts of PEDOT:PSS. This material is available free of charge via the Internet at http://pubs.acs.org.

■ AUTHOR INFORMATION

Corresponding Author

*E-mail: cuigl@qibebt.ac.cn.

Present Address

[⊥]University of Chinese Academy of Sciences, Beijing 100049, People's Republic of China.

Notes

The authors declare no competing financial interest.

■ ACKNOWLEDGMENTS

This work was supported by the National Program on Key Basic Research Project of China (973 Program; Grant MOST2011CB935700), the "100 talents" program of Chinese Academy of Sciences, the National Natural Science Foundation (Grants 20901044 and 20902052), and the Natural Science Foundation of Shandong Province (Grants ZR2009BM014 and ZR2010BM016).

■ REFERENCES

(1) O'Regan, B.; Grätzel, M. *Nature* **1991**, *353*, 737.
(2) Grätzel, M. *Nature* **2001**, *414*, 338.
(3) Yang, L.; Zhai, J.; Wang, D.; Chen, Y.; Jiang, L. *ACS Nano* **2010**, *4*, 887.
(4) Heng, L.; Wang, X.; Yang, N.; Zhai, J.; Wan, M.; Jiang, L. *Adv. Funct. Mater.* **2010**, *20*, 266.
(5) Hagfeldt, A.; Boschloo, G.; Sun, L.; Kloo, L.; Pettersson, H. *Chem. Rev.* **2010**, *110*, 6595.
(6) Zhao, Y.; Zhai, J.; He, J. L.; Chen, X.; Chen, L.; Zhang, L. B.; Tian, Y. X.; Jiang, L.; Zhu, D. B. *Chem. Mater.* **2008**, *20*, 6022.

(7) Ding, T.; Wang, F.; Song, K.; Yang, G. Q.; Tung, C. H. *J. Am. Chem. Soc.* **2010**, *132*, 1740.
(8) Papageorgiou, N.; Maier, W. F.; Grätzel, M. *J. Electrochem. Soc.* **1997**, *144*, 876.
(9) Hauch, A.; Georg, A. *Electrochim. Acta* **2001**, *46*, 3457.
(10) Papageorgiou, N.; Coordin, N. *Chem. Rev.* **2004**, *248*, 1421.
(11) Roy-Mayhew, J. D.; Bozym, D. J.; Punckt, C.; Aksay, I. A. *ACS Nano* **2010**, *4*, 6203.
(12) Trancik, J. E.; Barton, S. C.; Hone, J. *Nano Lett.* **2008**, *8*, 982.
(13) Joshi, P.; Zhang, L. F.; Chen, Q. L.; Galipeau, D.; Fong, H.; Qiao, Q. Q. *ACS Appl. Mater. Interfaces* **2010**, *2*, 3572.
(14) Bay, L.; West, K.; Winther-Jensen, B.; Jacobsen, T. *Sol. Energy Mater. Sol. Cells* **2006**, *90*, 341.
(15) Saito, Y.; Kitamura, T.; Wada, Y.; Yanagida, S. *Chem. Lett.* **2002**, *10*, 1060.
(16) Saito, Y.; Kubo, W.; Kitamura, T.; Wada, Y.; Yanagida, S. *J. Photochem. Photobiol. A* **2004**, *164*, 153.
(17) Wu, M. X.; Lin, X.; Hagfeldt, A.; Ma, T. L. *Angew. Chem., Int. Ed.* **2011**, *50*, 3520.
(18) Xu, H.; Zhang, X.; Zhang, C.; Liu, Z.; Zhou, X.; Pang, S.; Chen, X.; Dong, S.; Zhang, L.; Han, P.; Wang, X.; Cui, G. *ACS Appl. Mater. Interfaces* **2012**, *4*, 1087.
(19) Li, G. R.; Song, J.; Pan, G. L.; Gao, X. P. *Energy Environ. Sci.* **2011**, *4*, 1680.
(20) Wang, M.; Anghel, A. M.; Marsan, B.; Cevey Ha, N. L.; Pootrakulchote, N.; Zakeeruddin, S. M.; Grätzel, M. *J. Am. Chem. Soc.* **2009**, *131*, 15976.
(21) Sun, H. C.; Qin, D.; Huang, S. Q.; Guo, X. Z.; Li, D. M.; Luo, Y. H.; Meng, Q. B. *Energy Environ. Sci.* **2011**, *4*, 2630.
(22) Wu, M. X.; Wang, Y. D.; Lin, X.; Yu, N. S.; Wang, L.; Wang, L. L.; Hagfeidt, A.; Ma, T. L. *Chem. Chem. Phys.* **2011**, *13*, 19298.
(23) Zhong, X. H.; Feng, Y. Y.; Knoll, W.; Han, M. Y. *J. Am. Chem. Soc.* **2003**, *125*, 13559.
(24) Xin, X. K.; He, M.; Han, W.; Jung, J. H.; Lin, Z. Q. *Angew. Chem., Int. Ed.* **2011**, *50*, 11739−11742.
(25) Koo, B.; Patel, R. N.; Korgel, B. A. *Chem. Mater.* **2009**, *21*, 1962.
(26) Kruszynska, M.; Borchert, H.; Parisi, J.; Kolny-Olesiak, J. *J. Am. Chem. Soc.* **2010**, *132*, 15976.
(27) Zhong, H. Z.; Lo, S. S.; Mirkovic, T.; Li, Y. C.; Ding, Y. Q.; Li, Y. F.; Scholes, G. D. *ACS Nano* **2010**, *4*, 5253.